Reference-based MRI

Lior Weizman[a)] and Yonina C. Eldar
Department of Electrical Engineering, Technion - Israel Institute of Technology, Haifa 32000, Israel

Dafna Ben Bashat
Functional Brain Center, Tel Aviv Sourasky Medical Center, Sackler Faculty of Medicine and Sagol School of Neuroscience, Tel Aviv University, Tel Aviv 6997801, Israel

Purpose: In many clinical MRI scenarios, existing imaging information can be used to significantly shorten acquisition time or to improve Signal to Noise Ratio (SNR). In this paper the authors present a framework, referred to as FASTMER, for fast MRI by exploiting a reference image.

Methods: The proposed approach utilizes the possible similarity of the reference image to the acquired image, which exists in many clinical MRI imaging scenarios. Examples include similarity between adjacent slices in high resolution MRI, similarity between various contrasts in the same scan and similarity between different scans of the same patient. To account for the fact that the reference image may exhibit low similarity with the acquired image the authors develop an iterative weighted reconstruction approach, which tunes the weights according to the degree of similarity.

Results: Experimental results demonstrate the performance of the method in three different clinical MRI scenarios: The first example demonstrates SNR improvement in high resolution brain MRI, the second scenario exploits similarity between T2-weighted and fluid-attenuated inversion recovery (FLAIR) for fast FLAIR scanning and the last application utilizes similarity between baseline and follow-up scans for fast follow-up acquisition. The results show that FASTMER outperforms image reconstruction of existing state-of-the-art methods.

Conclusions: The authors present a framework for fast MRI by exploiting a reference image. Recovery is based on an iterative algorithm that supports cases in which similarity to the reference scan is not guaranteed. This extends the applicability of the FASTMER to different MRI scanning scenarios. Thanks to the existence of reference images in various clinical imaging tasks, the proposed framework can play a major role in improving reconstruction in many MR applications. © *2016 American Association of Physicists in Medicine.* [http://dx.doi.org/10.1118/1.4962032]

1. INTRODUCTION

Magnetic resonance imaging (MRI) data is sampled in the spatial Fourier transform (a.k.a. *k*-space) domain of the object under investigation. In many cases, the *k*-space is sampled below the Nyquist rate due to implementation constraints on the *k*-space trajectory that control the sampling pattern (e.g., acquisition duration and smoothness of gradients). Mostly, prior assumptions on the nature of the data are taken into account in the reconstruction process, to overcome imaging artifacts due to insufficient sampling. We can roughly divide MRI reconstruction approaches from undersampled *k*-space into two families: single- and multiple-image based recovery.

The first family of methods exploits prior assumptions on a single MR image, in order to improve its reconstruction from undersampled data. Since the introduction of Compressed Sensing (CS)[1–4] to the field of MRI,[5] many MRI reconstruction approaches exploit the fact that MR images are highly compressible, by formulating the image reconstruction problem as an ℓ_1 minimization problem. Wavelet transform sparsity has been widely used as a sparsifying transform for brain MRI. Total Variation (TV) is often used for MR images which are sparse in the image domain, such as angio-MRI.[5,6] Several

works use *a-priori* information to improve reconstruction of single-contrast MRI.[24–27] Other approaches focus on learning the sparsifying transform or using a dictionary developed exclusively for MRI.[7–9]

The second family of techniques exploit similarity to a single reference image or within a series of MR images. In Table I we present a concise review of prior art in methods that take advantage of reference images to speed-up acquisition or to improve image reconstruction. Most algorithms were applied to dynamic or Diffusion MRI, where multiple images are acquired at a single imaging session. This allows the exploitation of similarity along the temporal dimension, assuming that only parts of the field-of-view (FOV) change over time. State-of-the-art approaches use temporal similarity in various ways. They can be roughly divided into methods based on generalized reconstruction schemes,[10–14] Bayesian-based approaches,[15] CS-based methods[16–20] and techniques using low-rank properties.[21–23]

Additional works that exploit similarity in a series of MR images focus on structural MRI. In multiple-contrast MRI, structural similarity between different contrasts in the same scan is assumed and can be used to enhance reconstruction.[28–31] Another approach taken by several authors

TABLE I. Summary of related methods that exploit a reference image for fast MRI. Our proposed method is last in the table. Abbreviations used: DCE: dynamic contrast enhanced, CS: compressed sensing, DWI: diffusion weighted imaging, TV: total variation, fMRI: functional MRI.

Author	Description	Imaging application tested
Liang and Lauterbur (Ref. 44)	Exploiting temporal similarity in dynamic MRI using generalized scheme imaging	Dynamic MRI (dynamic T1-weighted and diffusion MRI)
Hanson et al. (Ref. 11)	Exploiting two high resolution reference images to improve dynamic imaging in a generalized scheme	Dynamic MRI (DCE MRI)
Hess et al. (Ref. 12)	Exploiting reference image for generation of basis functions, used to improve dynamic MRI	Dynamic MRI (MR angiography)
Tsao et al. (Ref. 32)	Incorporating reference image and prior on changed regions for improved reconstruction	Longitudinal MRI
Tsao et al. (Ref. 45)	Exploiting spatiotemporal correlations for dynamic MRI (training-based approach)	Dynamic MRI (cardiac imaging)
Lustig et al. (Ref. 16)	Random sampling in k-t space, reconstruction based on wavelet-Fourier sparsity	Dynamic MRI (cardiac imaging)
Haldar et al. (Ref. 46)	Using anatomical priors to improve SNR via penalized ML	Single-contrast MRI
Lang and Ji (Ref. 17)	Exploiting similarity to a reference image in a CS framework	Dynamic MRI (brain DCE)
Gamper et al. (Ref. 18)	Exploiting sparsity in the x-f space for dynamic MRI	Dynamic MRI (cardiac imaging)
Jung et al. (Ref. 19)	Exploiting sparsity of residuals in dynamic MRI	Dynamic MRI (cardiac imaging)
Yun et al. (Ref. 13)	Exploiting a reference image for basis functions generation used to improve dynamic MRI	Dynamic MRI (brain fMRI)
Samsonov et al. (Ref. 33)	Exploiting sparsity of gradient of difference between baseline and follow-up scans	Longitudinal MRI
Chen et al. (Ref. 20)	Exploring the exploitation of a reference frame in x-t and x-f domains in dynamic MRI	Dynamic MRI (cardiac imaging)
Wu et al. (Ref. 24)	Using noisy reconstruction as a reference for sorting in parallel imaging	Single-contrast MRI
Peng et al. (Ref. 25)	Exploiting reference image for sparsifying transform generation	Single-contrast MRI
Bilgic et al. (Ref. 28)	Exploit similarity of spatial derivatives in multicontrast MRI	Multicontrast MRI
Du and Lam (Ref. 26) and Lam et al. (Ref. 27)	Exploiting similarity to a reference image in a CS-based hybrid reconstruction and registration scheme	Single-contrast MRI
Nguyen and Glover (Ref. 14)	Exploiting a reference image for generation of basis functions used for generalized series reconstruction of dynamic MRI	Dynamic MRI (brain fMRI)
Haldar et al. (Ref. 15)	Using structural MRI for SNR improvement of DWI in an ML scheme	Diffusion MRI
Qu et al. (Refs. 29 and 30)	Exploiting similarity of image patches within and between multicontrast MRI in CS framework	Multicontrast MRI
Huang et al. (Ref. 31)	Joint TV and group wavelet based reconstruction for multicontrast MRI	Multicontrast MRI
Chiew et al. (Ref. 21)	Low-rank based reconstruction	Dynamic MRI (brain fMRI)
Li et al. (Ref. 34)	Using nonreference-based reconstruction as a prior for reference-based reconstruction	Longitudinal MRI
Adluru et al. (Ref. 22)	Exploiting TV-based reconstruction for improved low-rank based reconstruction	Dynamic MRI (cardiac imaging)
Otazo et al. (Ref. 23)	Low-rank based reconstruction	Dynamic MRI (cardiac imaging, MR angiography)
Our method (FASTMER)	Exploiting reference image in an adaptive-weighted CS scheme	Single- and Multicontrast MRI, Longitudinal MRI

is to exploit similarity in longitudinal MRI, where images were acquired at different time points.[32–34] Finally, the use of reference images to improve reconstruction has also been tested in other imaging modalities, such as Magnetic Resonance Spectroscopy (MRS),[10,35] Positron Emission Tomography (PET)[36–38] and X-Ray Computed Tomography (X-Ray CT).[39]

Taking a closer look at the rightmost column of Table I, we observe that multiple-image based reconstruction is application specific; since similarity between multiple images takes on different forms, a separate reconstruction approach was developed for each MRI application, exploiting its specific nature. No general sampling and reconstruction scheme which fits a variety of multiple-image MRI applications has been developed so far. Moreover, most of the methods rely on the assumption that there is substantial similarity between the

images in the series (e.g., dynamic imaging), in the image or in some transform domain. Assuming similarity of intensity between the reference image and the current scan may not always be valid (e.g., when a different imaging contrast is used as a reference or due to misalignment between images) and therefore may lead to undesired reconstruction results.

Recently, we introduced an iterative approach for sampling and reconstruction of multiple MRIs of the same patient by exploiting similarity between the images.[40] We considered the acquisition of a follow-up MRI, given the baseline scan of the same patient. Taking into account that baseline and follow-up images may not always exhibit similarity we developed a solution based on an iterative weighted mechanism. It adjusts the reconstruction parameters and the sampling locations during real-time scanning. While the idea of optimizing the

sampling locations has been previously proposed by others,[41] it suffers from practical difficulties due to the necessity to solve many computationally heavy ℓ_1 minimization problems during the acquisition process. In related work,[42] we have shown that enforcing similarity between adjacent, low SNR, thin MRI slices, can lead to significant improvement in SNR that obviates the need for multiple excitations in order to achieve high SNR.

In a recent conference paper we presented the initial concept of applying a reference-based approach for multiple MRI applications.[43] The conference paper includes an earlier version of the model described in this paper, with preliminary results obtained via retrospective two dimensional random sampling.

In this paper we present a framework to exploit a reference image that is applicable to various MRI applications. The major contributions of this paper are: (a) exploiting similarity of intensity values to a reference scan is performed in an adaptive and weighted fashion, taking into account that the reference may exhibit major gray-level differences with respect to the current scan and; (b) testing several MRI imaging applications (single-contrast high resolution MRI, multicontrast MRI, and longitudinal MRI), with 2D radial sampling.

More specifically, we introduce a framework, called FAST MRI by Exploiting a Reference scan (FASTMER) which is based on two main elements: (a) taking advantage of both sparsity in the wavelet domain and similarity to a reference scan and (b) weighted reconstruction by adaptive selection of weights during the reconstruction process, taking into account the degree of similarity to the reference image. The adaptive weights adjust the reconstruction to the actual similarity between the scans. Therefore, it fits a variety of clinical imaging applications that can be improved with supplemental imaging information, which is often neglected due to its low fidelity.

Experimental results demonstrate the applicability of the proposed method in three different MRI applications that utilize similarity to a reference image. The first application exploits similarity between two different imaging contrasts for fast scanning of one of them. The second example utilizes similarity between different scans of the same patient for fast scanning of follow-up scans, and the third application takes advantage of similarity between adjacent slices to improve SNR within the same imaging contrast.

The paper is organized as follows. Section 2 presents the proposed reference-based MRI approach. Section 3 develops an extension of the approach for improving SNR in adjacent, low SNR MRI slices. Section 4 describes experimental results. Section 5 discusses theoretical aspects and implementation details of FASTMER and Sec. 6 concludes by highlighting the key results.

2. REFERENCE-BASED MRI

2.A. Compressed Sensing MRI

The application of CS for MRI (Ref. 5) exploits the fact that MRI scans are typically sparse in a transform domain, which is incoherent with the sampling domain.

Nonlinear reconstruction is then used to enforce both sparsity of the image representation in some transform domain and consistency with the acquired data. A typical formulation of CS MRI recovery aims to solve the following unconstrained optimization problem (in a so-called Lagrangian form):

$$\min_{\mathbf{x}} \quad \|\mathbf{F}_u\mathbf{x} - \mathbf{y}\|_2^2 + \lambda\|\mathbf{\Psi}\mathbf{x}\|_1, \tag{1}$$

where $\mathbf{x} \in \mathbb{C}^N$ is the N-pixel complex image to be reconstructed, represented as a vector, $\mathbf{y} \in \mathbb{C}^M$ denotes the k-space measurements, $\mathbf{F}_u$ is the undersampled Fourier transform operator, $\mathbf{\Psi}$ is a sparsifying transform operator and λ is a properly chosen regularization parameter. We focus on brain MRI, known to be sparse in the wavelet domain. Therefore, we will assume throughout that $\mathbf{\Psi}$ is an appropriately chosen wavelet transform.

This fundamental CS MRI formulation is the basis for many MRI reconstruction applications, where the sparse transform domain varies depending on the particular setting.[16–19] We note that this formulation does not take into account any image-based prior information, that exists in many MRI applications.

2.B. Reference-based compressed sensing MRI

In many MRI imaging scenarios, an *a-priori* image that may exhibit similarity to the acquired image, is available. This image is coined hereinafter the "reference image" and represented by $\mathbf{x}_0$. A reference image could be a different imaging contrast in the same scan, an adjacent image slice or a previous scan of the same patient.

In some imaging applications, we may assume that $\mathbf{x}_0$ and $\mathbf{x}$ are similar in most image regions.[18] Therefore the difference $\mathbf{x} - \mathbf{x}_0$ can be modeled as sparse, and a CS based optimization may utilize the reference image for improved reconstruction, via ℓ_1 minimization. Such reference-based CS takes into account the fidelity of the measurements and the similarity to the reference scan, as follows:

$$\min_{\mathbf{x}} \quad \|\mathbf{F}_u\mathbf{x} - \mathbf{y}\|_2^2 + \lambda\|\mathbf{x} - \mathbf{x}_0\|_1. \tag{2}$$

This optimization problem assumes high degree of similarity between $\mathbf{x}_0$ and $\mathbf{x}$, and is therefore suitable for some specific MRI applications, such as dynamic MRI. However, many MRI applications do not utilize available reference imaging information [for instance, by solving Eq. (2)] due to the fact that the similarity to the acquired image is partial, not guaranteed or unknown.

We introduce a framework for reference based MRI, which takes into account the fact that $\mathbf{x}_0$ may exhibit differences versus $\mathbf{x}$. We also account for the fact that the vector $\mathbf{y}$ may represent multiple images that are contaminated with noise at different levels; we want to prioritize images with low noise standard deviation over ones with high noise standard deviation in the reconstruction process. Our approach is based on enforcing similarity between $\mathbf{x}$ and $\mathbf{x}_0$ via a weighted ℓ_1 norm:

$$\min_{\mathbf{x}} \|\mathbf{A}(\mathbf{F}_u\mathbf{x} - \mathbf{y})\|_2^2 + \lambda_1\|\mathbf{W}_1\mathbf{\Psi}\mathbf{x}\|_1 + \lambda_2\|\mathbf{W}_2(\mathbf{x} - \mathbf{x}_0)\|_1 \tag{3}$$

where $\mathbf{A}$ is a diagonal matrix that controls the weight given to the fidelity of certain measurements (used to prioritize

samples taken from images with low noise standard deviation). The matrices $\mathbf{W}_1$ and $\mathbf{W}_2$ are weighting matrices, $\mathbf{W}_k = \mathrm{diag}([w_k^1, w_k^2, \ldots, w_k^N])$ with $0 \le w_k^i \le 1$, that control the weight given to each element in the sparse representation. In particular, $\mathbf{W}_1$ is used to weight specific wavelet atoms in the reconstruction process and $\mathbf{W}_2$ is used to weight image regions according to their similarity level with the reference scan. The parameters λ_1 and λ_2 are regularization parameters that control the weight given to each term in the optimization problem.

In most cases, the expected noise level of the acquired data is known and the matrix $\mathbf{A}$ can be determined in advance. As to $\mathbf{W}_1$ and $\mathbf{W}_2$, there are cases in which neither the similarity to the reference image nor the support in the wavelet domain are known in advance. Therefore, we suggest determining these matrices during the recovery process, as described in the next section.

2.C. Adaptive weighting for reference based MRI

Since the similarity of $\mathbf{x}$ to $\mathbf{x}_0$, as well as the support of $\mathbf{x}$ in the wavelet domain, are unknown, we estimate the matrices $\mathbf{W}_1$ and $\mathbf{W}_2$ from the acquired data, in an adaptive fashion. Inspired by Weighted-CS,[47] we propose an iterative reconstruction algorithm, where in each iteration a few k-space samples are added to the reconstruction process, based on their distance from the origin of the k-space (samples closer to the origin of the k-space are added first). The rationale lies in the structure of the minimization problem (3). Due to the fact that Eq. (3) is a nonconvex minimization problem, we would like to avoid convergence to local minima. Experimentally we observed that gradually adding k-space samples at each iteration leads to more rapid convergence and improved results. At the end of each iteration, $\hat{\mathbf{x}}$ is estimated, and serves as the basis for estimating the weighting matrices in the next iteration.

The motivation for the iterative computation of $\mathbf{W}_k$ is as follows. For $\mathbf{W}_1$, we would like to relax the demand for sparsity on elements in the support of $\mathbf{\Psi}\mathbf{x}$. For $\mathbf{W}_2$, we would like to enforce sparsity only in spatial regions where $\mathbf{x} \approx \mathbf{x}_0$. When one of the weights takes on a small value, for instance, $w_2^i \to 0$, then the sparsity on the corresponding image pixel, $\mathbf{x}_i$, is relaxed, and vice-versa; when $w_2^i \to 1$, sparsity is enforced on $\mathbf{x}_i$ (i.e., the ℓ_1 minimization will prefer solutions where $\mathbf{x}_i \to 0$).

Since $\mathbf{x}$ is unknown, $\hat{\mathbf{x}}$, updated in every iteration, is used instead. The elements of the weighting matrices are then chosen as follows:

$$w_1^i = \frac{1}{1 + [|\mathbf{\Psi}\hat{\mathbf{x}}|]_i}$$
$$w_2^i = \frac{1}{1 + [|\hat{\mathbf{x}} - \mathbf{x}_0|]_i} \tag{4}$$

where $[\cdot]_i$ denotes the ith element of the vector in brackets. Note that the weights in Eq. (4) vary between 0 and 1. The values for w_1^i and w_2^i are inversely proportional to those of the corresponding elements in the vectors $\mathbf{\Psi}\mathbf{x}$ and $\hat{\mathbf{x}} - \hat{\mathbf{x}}_0$, respectively. Therefore, since we expect the reconstruction quality to improve at each consecutive iteration, we obtain $w_2^i \to 1$ in regions where $\mathbf{x} \sim \mathbf{x}_0$, thereby enforcing sparsity of

---

ALGORITHM I. Fast MRI by Exploiting Reference (FASTMER).

Input:
  Number of iterations: N_I
  Reference image: $\mathbf{x}_0$
  Sampled k-space: $\mathbf{z}$
  Tuning constants: λ_1, λ_2
  Number of k-space samples added at each iteration: N_k
  Expected fidelity of measurements: $\mathbf{A}$
Output: Estimated image: $\hat{\mathbf{x}}$
Initialize:
  $\mathbf{W}_1 = \mathbf{I}$, $\mathbf{W}_2 = \mathbf{0}$
Reconstruction:
  for $l = 1$ to N_I **do**
  Add N_k new samples to $\mathbf{y}$ from $\mathbf{z}$ according to distance from center of k-space
  Weighted reconstruction: Estimate $\hat{\mathbf{x}}$ by solving Eq. (3)
  Update weights: Update $\mathbf{W}_1$ and $\mathbf{W}_2$ according to Eq. (4)
  end for

---

the difference $\mathbf{x} - \mathbf{x}_0$ in those regions. The same analysis applies to $\mathbf{W}_1$ and the representation of the image in the wavelet domain.

The proposed algorithm is coined FAST MRI by Exploiting a Reference scan (FASTMER) and is summarized in Algorithm I. Note that in the first iteration of the algorithm we do not assume similarity with the reference image (i.e., we set $\mathbf{W}_1 = \mathbf{I}$ and $\mathbf{W}_2 = \mathbf{0}$). This is done in order to prevent the algorithm from convergence to an incorrect solution in cases where similarity between scans does not exist.

To solve the ℓ_1-minimization problem (3) in the weighted reconstruction phase, we use an extension of SFISTA.[48] The extended algorithm is summarized in Algorithm II, where the notation $\|\cdot\|_2$ for matrices denotes the largest singular value. The operator $\Gamma_{\lambda\mu}(\mathbf{z})$ is the soft shrinkage operator, which is applied element-wise on $\mathbf{z}$ and is defined as (for complex

---

ALGORITHM II. SFISTA algorithm for FASTMER.

Input:
  k-space measurements: $\mathbf{y}$
  Sparsifying transform operator: $\mathbf{\Psi}$
  An $N \times N$ k-space undersampling operator: $\mathbf{F}_u$
  Reference image: $\mathbf{x}_0$
  Expected fidelity of measurements: $\mathbf{A}$
  Tuning constants: $\lambda_1, \lambda_2, \mu$
  An upper bound: $L \ge \|\mathbf{A}\mathbf{F}_u\|_2^2 + \frac{\|\mathbf{W}_1\mathbf{\Psi}\|_2^2 + \|\mathbf{W}_2\|_2^2}{\mu}$
Output: Estimated image: $\hat{\mathbf{x}}$
Initialize:
  $\mathbf{x}_1 = \mathbf{z}_2 = \mathbf{F}_u^*\mathbf{y}$, $t_2 = 1$
Iterations:
  Step k:$(k \ge 2)$ Compute
  $\nabla f(\mathbf{z}_k) = \mathbf{A}^*(\mathbf{F}_u^*(\mathbf{A}(\mathbf{F}_u\mathbf{z}_k - \mathbf{y})))$
  $\nabla g_{1\mu}(\mathbf{W}_1\mathbf{\Psi}\mathbf{x}_{k-1}) = \frac{1}{\mu}\mathbf{W}_1\mathbf{\Psi}^*(\mathbf{W}_1\mathbf{\Psi}\mathbf{x}_{k-1} - \Gamma_{\lambda_1\mu}(\mathbf{W}_1\mathbf{\Psi}\mathbf{x}_{k-1}))$
  $\nabla g_{2\mu}(\mathbf{W}_2(\mathbf{x}_{k-1} - \mathbf{x}_0)) = \frac{1}{\mu}\mathbf{W}_2(\mathbf{W}_2(\mathbf{x}_{k-1} - \mathbf{x}_0) - \Gamma_{\lambda_2\mu}(\mathbf{W}_2(\mathbf{x}_{k-1} - \mathbf{x}_0)))$
  $\mathbf{x}_k = \mathbf{z}_k - \frac{1}{L}(\nabla f(\mathbf{z}_k) + \nabla g_{1\mu}(\mathbf{W}_1\mathbf{\Psi}\mathbf{x}_{k-1}) + \nabla g_{2\mu}(\mathbf{W}_2(\mathbf{x}_{k-1} - \mathbf{x}_0)))$
  $t_{k+1} = \frac{1 + \sqrt{1 + 4t_k^2}}{2}$

valued z_i):

$$\Gamma_{\lambda\mu}(z_i) = \begin{cases} \frac{|z_i| - \lambda\mu}{|z_i|} z_i, & |z_i| > \lambda\mu \\ 0, & \text{otherwise.} \end{cases} \quad (5)$$

Algorithm II minimizes Eq. (3), where the trade-off between the two sparsity assumptions is controlled by the ratio between λ_1 and λ_2, via $\Gamma(\cdot)$, and the overall convergence is controlled by μ.

3. FASTMER FOR SNR IMPROVEMENT

In MRI, SNR is proportional to the number of protons involved in generating the measured signal. As a result, thick slices provide better SNR than thin ones. However, the thinner the slice, the better the image resolution in the z-axis. Therefore, to obtain high quality MRI for clinical evaluation purposes, high SNR MRI that consists of thin slices is required. The common approach today for SNR improvement of MRI with thin slices consists of averaging over several excitations (usually three or four), which extends the scanning time by the same amount.

In this application, where thin slices are acquired, one may consider shortening scanning time by reducing the number of excitations and exploiting similarity between thin slices. In addition, similarity to a thick, high SNR image slice that overlaps the thin slices can also be utilized for SNR improvement.

We will consider a specific implementation, where a single excitation is used to acquire two thin adjacent slices with low SNR, $\mathbf{x}_1$ and $\mathbf{x}_2$, and a single thick slice, $\mathbf{x}_3$ that spatially overlaps $\mathbf{x}_1$ and $\mathbf{x}_2$. Our goal is to improve the SNR of $\mathbf{x}_1$ and $\mathbf{x}_2$ taking into account the similarity between them and the high-SNR, thick slice, $\mathbf{x}_3$. In this specific example we perform a total of three acquisitions for high SNR reconstruction of two adjacent slices, instead of 8 acquisitions (4 excitations for each thin slice) in the conventional, multiple excitations-based approach.

To introduce the method within our framework, let

$$\mathbf{y} = \begin{bmatrix} \mathbf{y}_1 \\ \mathbf{y}_2 \\ \mathbf{y}_3 \end{bmatrix}, \qquad \mathbf{x} = \begin{bmatrix} \mathbf{x}_1 \\ \mathbf{x}_2 \\ 0.5(\mathbf{x}_1 + \mathbf{x}_2) \end{bmatrix} \quad (6)$$

where $\mathbf{y}$ represents the k-spaces of two thin slices and the corresponding thick one, respectively, and $\mathbf{x}$ represents the two thin slices and their average, which corresponds to the overlapping thin slice. The matrix $\mathbf{A}$ is determined by the estimated noise level of the elements in $\mathbf{y}$, such that $\mathbf{A} = \text{diag}(^1/\sigma_1\mathbf{I}_N, ^1/\sigma_2\mathbf{I}_N, ^1/\sigma_2\mathbf{I}_N)$ where $\{\sigma_i\}_{i=1}^3$ are the noise standard deviations of $\{\mathbf{y}_i\}_{i=1}^3$, respectively and $\mathbf{I}_N$ is an identity matrix of size N. Similarity is enforced between the thin slices, and Eq. (3) is reformulated as:

$$\min_{\mathbf{x}} \|\mathbf{A}(\mathbf{F}_3\mathbf{x} - \mathbf{y})\|_2^2 + \lambda_1\|\mathbf{W}_1\mathbf{\Psi}_3\mathbf{x}\|_1 + \lambda_2\|\mathbf{W}_2\mathbf{B}\mathbf{x}\|_1. \quad (7)$$

Here $\mathbf{F}_3 = \text{diag}([\mathbf{F},\mathbf{F},\mathbf{F}])$ is a block diagonal matrix, with three Fourier matrices on the main diagonal, $\mathbf{\Psi}_3 = \text{diag}([\mathbf{\Psi},\mathbf{\Psi},\mathbf{\Psi}])$ and $\mathbf{B} = [\mathbf{I}_N \quad -\mathbf{I}_N \quad \mathbf{0}]$.

Similarity between the thick slice to the average between the thin slices is enforced in the Fourier domain, via the leftmost term of Eq. (7). Adapting Algorithms I and II to solve Eq. (7) is straightforward; the final method appears in Appendix A.

4. EXPERIMENTAL RESULTS

To demonstrate the performance of our reference based MRI approach we examine three MRI applications, all of which exploit a reference scan for improved reconstruction. For high quality ground truth reconstruction, the k-space was fully sampled with Cartesian sampling. Where relevant, partial acquisition was simulated by interpolation of radial k-space data (with angles selected randomly) from the fully sampled Cartesian k-space data. Nonuniform sampling and reconstruction was performed using the nonuniform Fourier transform (NUFFT) package of Fessler et al.[49] A Daubechies-4 wavelet transform was chosen as the sparsifying transform. Different values of λ_1, λ_2 in the range of [0, 0.9] were examined, and the best result in terms of image quality is presented in each case (see Sec. 4.D). We used $\mu = 10^{-3}(\lambda_1 + \lambda_2/2)^{-1}$ in our experiments. The number of iterations used in Algorithm II for the results obtained in this section is between 30 and 50.

All scans were performed on a GE Signa 1.5 T HDx scanner, using a 8-channel head coil with matrix size 320×320 and FOV of 20 cm for each in-plane direction. High SNR images reconstructed from fully sampled, multiple excitations data serve as the gold standard. The source code and data required to reproduce the results presented in this paper can be downloaded from: http://www.technion.ac.il/~weizmanl/software.

To provide a quantitative measure for the results, we examine the peak signal-to-noise ratio (PSNR) of each experiment, defined as: $\text{PSNR} = 10\log_{10}(M^2/V_s)$, where M denotes the maximum possible pixel value in the image and V_s is the Mean Squared Error (MSE) between the original image, $\mathbf{x}$ and the reconstructed image, $\hat{\mathbf{x}}$. The resulting weighting matrices ($\mathbf{W}_1$ and $\mathbf{W}_2$) are presented in Appendix B, as well as the similarity maps between the reference image and the reconstructed image.

Since the proposed approach is based on the difference between the reference image from the reconstruction, we need to verify that both images are aligned and have matched intensities. In the experiments presented hereinafter we conducted a wavelet-based reconstruction first [according to Eq. (1)] using the acquired data, to get a rough estimate of the alignment parameters and the gray-level range of the reconstructed image. Then, we embedded the extracted parameters in our reconstruction process for successful reference-based recovery. This issue is further discussed in Sec. 5.C.

4.A. Utilizing similarity between T2-weighted and FLAIR

In this experiment, our goal is to reconstruct a FLAIR image, $\mathbf{x}$, from undersampled measurements, utilizing similarity to a T2-weighted image. Images were acquired with slice thickness of 4 mm. FLAIR acquisitions parameters

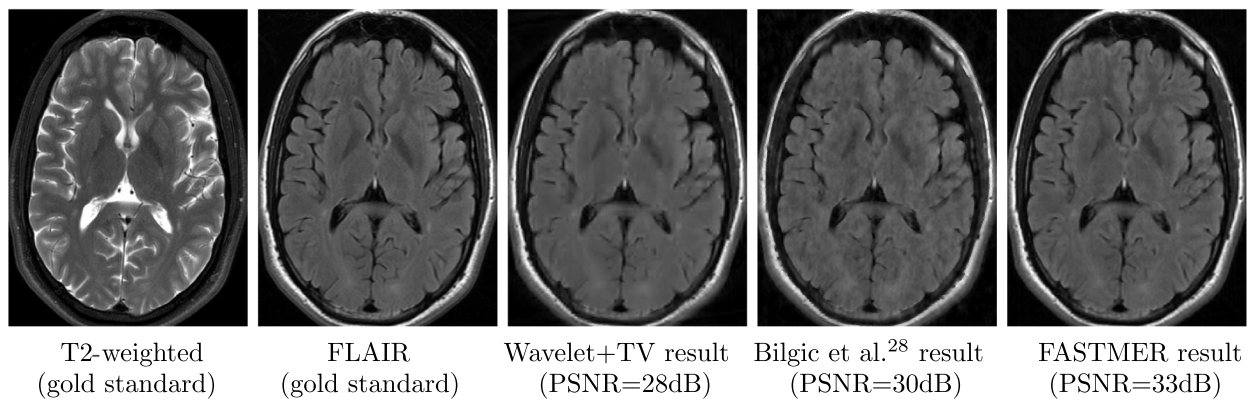| T2-weighted (gold standard) | FLAIR (gold standard) | Wavelet+TV result (PSNR=28dB) | Bilgic et al.[28] result (PSNR=30dB) | FASTMER result (PSNR=33dB) |

FIG. 1. FASTMER used within the same scan: reconstruction results utilizing similarity between T2 and FLAIR contrasts. The two leftmost images are the T2 and FLAIR images reconstructed from 100% of *k*-space data. The three rightmost images show reconstruction results from 25% of *k*-space FLAIR data, for wavelet+TV based reconstruction, the method of Bilgic *et al.* for multicontrast reconstruction using Bayesian-CS (Ref. 28) and our proposed, reference-based approach (FASTMER). The numbers in brackets are the PSNR values vs the FLAIR gold standard.

were: TE = 123 ms, TR = 8000 ms and TI = 2000 ms, and T2-weighted acquisition parameters were: TE = 68.4 ms and TR = 6880 ms. We sampled only 25% of the FLAIR *k*-space with radial sampling and utilized the fully sampled T2-weighted scan as the reference image $\mathbf{x}_0$. Since all samples were acquired with similar noise level, $\mathbf{A} = \mathbf{I}$.

To provide a baseline for comparison, we compared FASTMER to two methods. The first is reconstruction based on sparsity in the wavelet domain and enforces total-variation (wavelet+TV)[5] using undersampled FLAIR data only. The second is the algorithm of Bilgic *et al.*[28] which exploits the similarity of gradients between different contrasts.

Figure 1 shows the fully sampled T2 and FLAIR images, the wavelet+TV based reconstruction, reconstruction using the method of Bilgic *et al.*[28] and the result of FASTMER. In addition, the PSNR values of each method vs the gold-standard are provided. It can clearly be seen that FLAIR reconstruction with FASTMER outperforms the two other methods, using only 25% of the data.

4.B. Utilizing similarity between baseline and follow-up scans

Repeated brain MRI scans of the same patient every few weeks or months are very common for follow-up of brain tumors. Here, our goal is to use a previous scan in the time series as a reference scan for reconstruction of a follow-up scan. In this application we need to take into account that similarity between the reference and current scans is not guaranteed (e.g., due to pathology changes), and prior information on spatial regions that may exhibit differences is not available. These obstacles are discussed thoroughly in our previous publication[40] and in Sec. 5.C and Appendix C of this paper. Since all samples are acquired with similar noise level, we set $\mathbf{A} = \mathbf{I}$.

We compared FASTMER to two methods. The first is wavelet+TV based reconstruction. The second is the algorithm of Samsonov *et al.*[33] which exploits the gradient images similarity between a follow-up scan and a baseline scan using Bayesian-CS, in a nonweighted approach.

Figure 2 shows reconstruction results of a follow-up contrast enhanced T1-weighted brain scan utilizing the baseline scan as reference (TE = 11.5 ms, TR = 520 ms slice thickness: 1 mm for both scans). Results were obtained using only 25% of *k*-space data. It can be seen that FASTMER reveals imaging features that are hardly visible in both of the methods it is compared against. In addition, the PSNR values of each reconstruction algorithm vs the gold-standard are provided. The superiority of our approach is achieved thanks to the iterative mechanism that adapts the reconstruction to match actual similarity.

4.C. Utilizing similarity between adjacent slices

In our final application we examine the extension of fast reference based MRI detailed in Sec. 3 to improve SNR of thin MRI slices. We acquired a brain T2-weighted scan with slice thickness of 0.8 mm followed by an additional acquisition with slice thickness of 1.6 mm (TE = 68.4 ms and TR = 6880 ms for all scans). In all scans a single excitation was used. As a result, we obtained a low SNR scan consisting of thin slices, and high SNR scan consisting of thick slices where each thick slice overlaps two thin ones. Our goal is to reconstruct a high SNR scan comprised of thin slices from this data.

Figure 3 shows thin slices acquired using 4 excitations (NEX = 4), used as our gold standard in this experiment, and the noisy input images that were acquired with a single excitation (NEX = 1). Here, we compare our method to a wavelet+TV based approach, which has been tested previously to improve SNR in MRI.[6]

In terms of scanning time, 4 excitations are required to obtain thin slices with SNR comparable to SNR of data reconstructed with FASTMER. Therefore, without additional acceleration techniques (parallel imaging etc.), our approach requires scanning 3 slices once versus scanning 2 slices 4 times in conventional scanning, yielding a speed-up factor of 2.6.

4.D. Parameter sensitivity analysis

In this analysis we examine the sensitivity of FASTMER to changes in the regularization parameters of the algorithm.
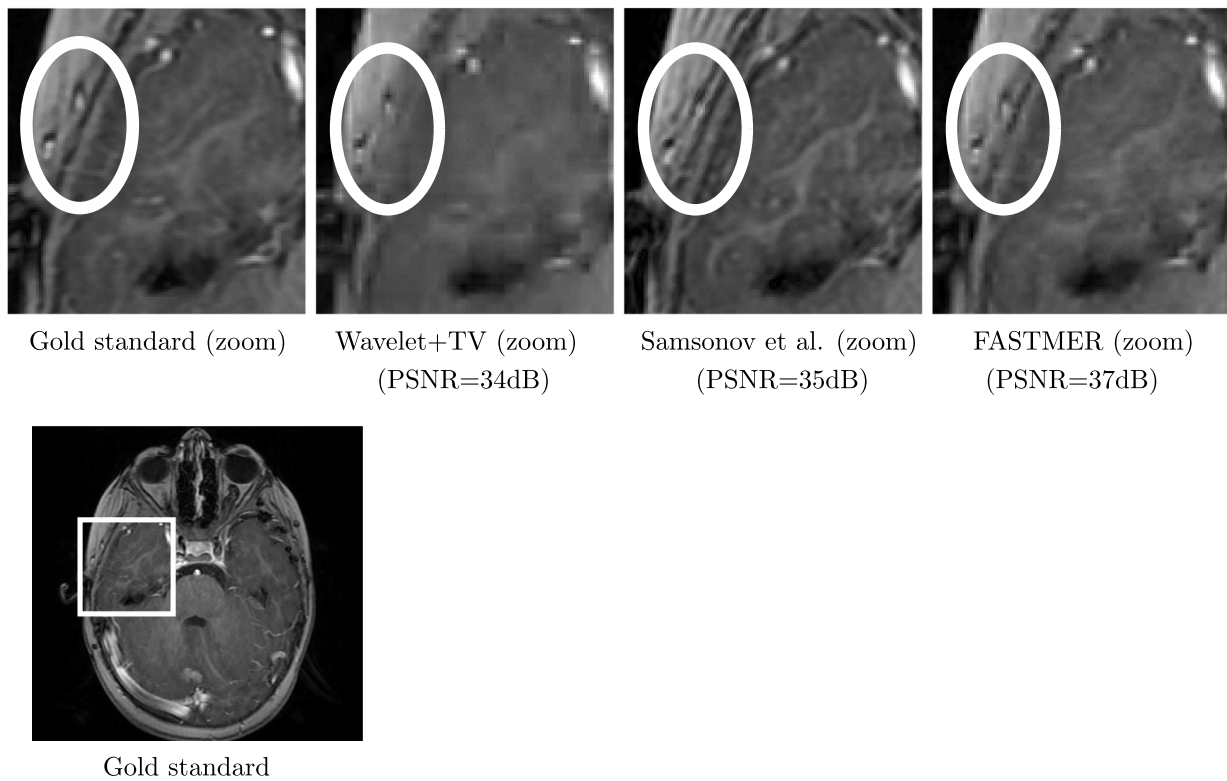
Gold standard (zoom)   Wavelet+TV (zoom)   Samsonov et al. (zoom)   FASTMER (zoom)
(PSNR=34dB)   (PSNR=35dB)   (PSNR=37dB)

Gold standard

FIG. 2. FASTMER used in longitudinal studies: reconstruction results from 25% of k-space data. Bottom left: ground truth follow-up image reconstructed from 100% of k-space data. The rectangle defines the region-of-interest explored in this figure. Upper row: Enlarged versions of the region-of-interest in the ground truth image (leftmost image), followed by the results of wavelet+TV based reconstruction, the method of Samsonov *et al.* for longitudinal studies (Ref. 33) and our proposed, reference-based approach (FASTMER). The numbers in brackets are the PSNR values vs the gold standard. It can be seen that FASTMER exhibits results which are very similar to the gold standard, and reveals imaging features that are blurred or not visible in other recoveries.

Figure 4 shows the PSNR results as λ_1 and λ_2 vary. The values shown for the adjacent slices experiment were averaged over the two thin slices used. Generally, we observe that lower values of λ_1 and λ_2, with $\lambda_1 < \lambda_2$ provide reasonable PSNR. This can be explained by the fact that over-promoting sparsity versus consistency to measurements degrades the reconstruction quality. In addition, we see that the T2-FLAIR experiment provides a lower range of PSNR values in comparison to other experiments. This can be explained by the fact that similarity is not enforced over the entire image in this case, due to many regions of differences between FLAIR and T2.

5. DISCUSSION

5.A. Theoretical justification

The algorithm presented in our paper generalizes the reweighted ℓ_1 minimization method by Candès, Wakin, and Boyd[47] to the case where there is side information (the reference-image in FASTMER). Their algorithm is intuitive, works very well in practice, and comes with analytical performance guarantees. In recent work, we have extended their theoretical analysis to our setting.[50] In particular, we developed a bound on the number of measurements required for perfect reconstruction of **x** with high probability in the presence of a reference. We also show that adding weights highly improves the results in comparison to other nonweighted ℓ_1-minimization based solutions.

5.B. Adaptive sampling and NUFFT

In our approach all data is acquired at once. Several recent publications suggest that prior knowledge can also be used to optimize data acquisition.[51–53] However, since in our framework the similarity between scans is not guaranteed, we avoid using prior information during sampling. Another way of utilizing the reference image in the sampling stage would be to acquire a small number of samples in each iteration based on the reconstruction results, in an adaptive manner.[41,54–57] This approach, which requires image reconstruction at each iteration as part of the sampling process, has been tested in our previous work.[40] It was shown to be time consuming leading to substantial increase of scanning time if not programmed in hardware or accelerated by other means.

Another issue related to sampling in our approach is the off grid sampling performed in our simulations. As opposed to our previous publications[40,42,43] that dealt with sampling locations on the k-space grid and FFT for reconstruction, in this paper we used radial sampling and the NUFFT for reconstruction. Although radial sampling reflects a realistic
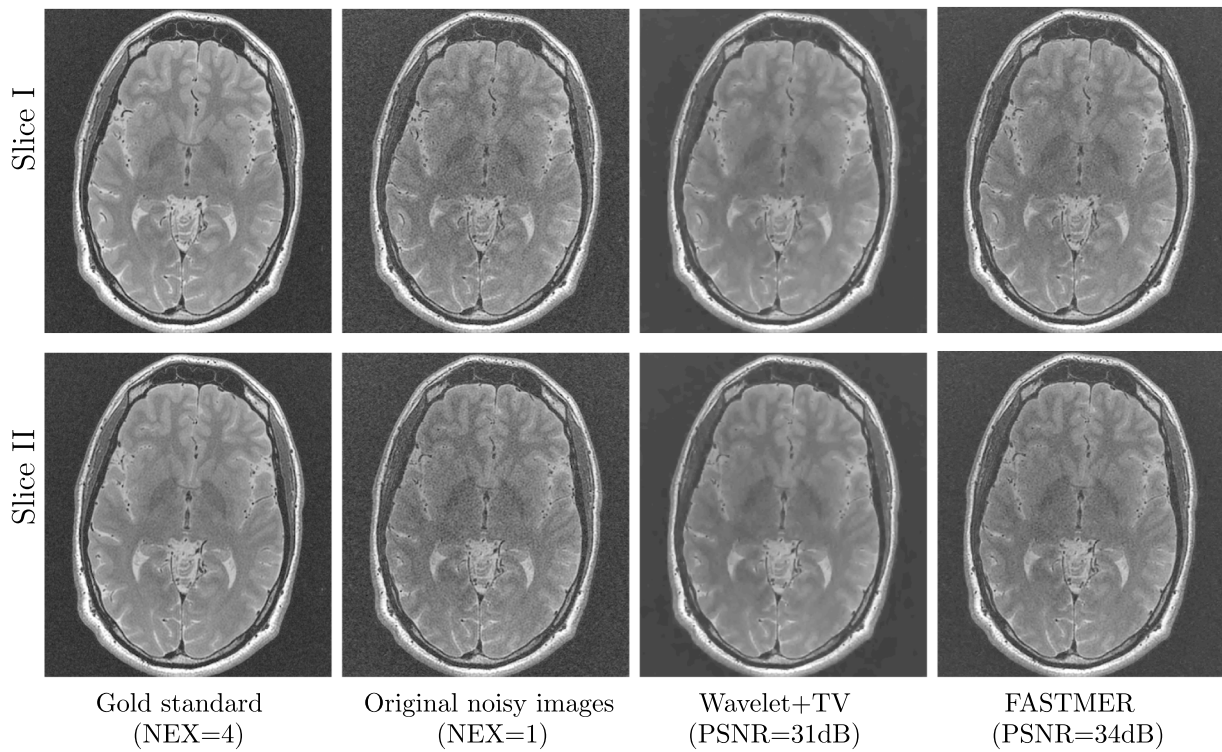
FIG. 3. FASTMER used within the same imaging contrast: reconstruction results from low SNR data. Each row corresponds to a single slice, from two adjacent slices. It can be seen that high similarity exists within adjacent slices, which can be exploited to improve SNR. The left most column shows the gold standard, acquired using four excitations (NEX=4). The input to our approach is presented as the original noisy images, acquired with single acquisition (NEX=1), followed by the result of a Total-Variation (TV)-based reconstruction. The rightmost column shows FASTMER recovery. The numbers in brackets are the PSNR values vs the gold standard (values were averaged over the two slices used in the experiment).

scenario for 2D, using NUFFT in the reconstruction requires increasing the sampling ratio to obtain results comparable to those obtained via Cartesian sampling and FFT. While only 15% of data was required in our previous publication[43] for adequate results in the T2-FLAIR experiment, the radial trajectories and NUFFT in this paper require 25% of the data for similar results. In addition, we need to take into account that NUFFT requires gridding and weighting processes, which increase the complexity of the transformation from $O(n\log n)$ in FFT, to $O(n^2)$ and more, depending on the algorithm used.[58]

5.C. Practical limitations

FASTMER provides the best results when the reference scan and the acquired scan are spatially aligned and exhibit

a similar range of gray-level intensities. While these assumptions are mostly valid within the same imaging contrast (our slice similarity application), they may not be valid for different contrasts or scans acquired at different times.

The solution to both issues can be obtained by gray-level normalization and realigning after acquisition. Since all data is acquired prior to reconstruction, a wavelet based recovery using all samples can be performed first. Although it may exhibit poor reconstruction of fine details (as presented in our experiments), it was found to be sufficient for gray-level normalization and alignment parameter extraction. Then, the extracted parameters are used for normalization and realignment of the data to improve reconstruction performance. An additional approach that is currently left for future research is to examine more complex similarity measures (in contrast
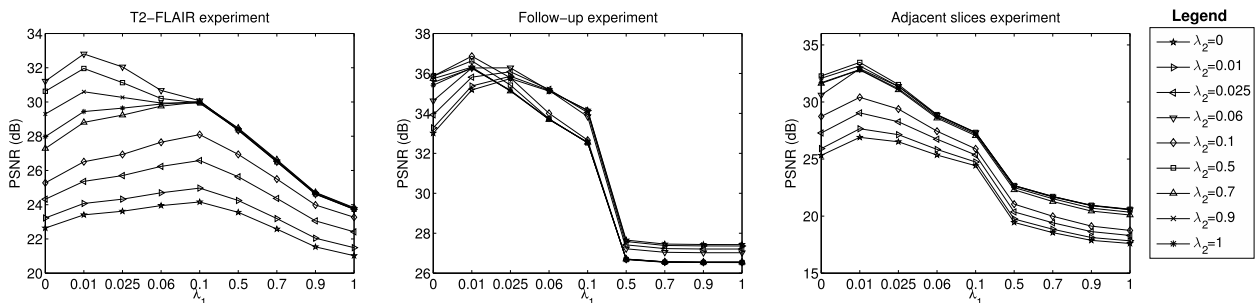

FIG. 4. Sensitivity analysis: PSNR results of T2-FLAIR (left), follow-up (middle) and adjacent slice similarity (top) applications for various values of λ_1 and λ_2. Each line represents a different value of λ_2, according to the legend on the left.

to the gray-level subtraction proposed in this paper), e.g., nonlinear similarity measures or measures that also take into account misalignment and intensity variation between the images. However, the solution to the corresponding ℓ_1 minimization problem with a nonlinear constraint might be more complex than FASTMER.

It is worth noting here that if the alignment and normalization processes fail, then our iterative approach will detect low similarity between the scans. As a result, the reference image will not be taken into account and the reconstructed image will converge to a wavelet-based reconstruction. This statement is supported by experiments presented in Appendix C.

6. CONCLUSIONS

In this paper we introduced a new framework: fast MRI by exploiting a reference image (FASTMER). We developed an iterative reconstruction approach that supports cases in which similarity to the reference scan is not guaranteed. While the issue of embedding prior images in MRI reconstruction to accelerate acquisition and improve SNR has been examined in the past, in this paper the similarity to the reference image is learned during reconstruction. As a result, data that is not similar is ignored in the reconstruction process, which enables the applicability of the method to a variety of MRI applications.

We demonstrate the performance of our framework in three clinical MRI applications: Reconstruction of noisy, single-contrast data, multicontrast recovery and longitudinal reconstruction. Results exhibit significant improvement versus wavelet+TV based reconstruction and other MRI application-specific approaches.

Thanks to the existence of reference images in various clinical imaging scenarios, the proposed framework can play a major part in improving reconstruction in many MR applications. In future work it would be interesting to apply the method to a wider range of medical imaging settings, such as low dose CT and fMRI, as well as to explore the combination of CS for parallel imaging and the proposed approach.

ACKNOWLEDGMENTS

CONFLICT OF INTEREST DISCLOSURE

The authors have no COI to report.

APPENDIX A: ADAPTATION OF ALGORITHM I AND II FOR REFERENCE-BASED SNR IMPROVEMENT

The SNR improvement in Sec. 3 requires the solution of Eq. (7) in an iterative manner. For this purpose, we define the weights update as follows:

$$w_1^i = \frac{1}{1 + [|\mathbf{\Psi}_3\hat{\mathbf{x}}|]_i}$$
$$w_2^i = \frac{1}{1 + [|\mathbf{B}\hat{\mathbf{x}}|]_i}. \tag{A1}$$

Below we describe Algorithms III and IV, which are adaptations of Algorithms I and II to this setting, where $\Gamma_{\lambda\mu}(\mathbf{z})$ is defined in Eq. (5), $\mathbf{F}_3^* = \text{diag}([\mathbf{F}^*,\mathbf{F}^*,\mathbf{F}^*])$ and $\mathbf{\Psi}_3^* = \text{diag}([\mathbf{\Psi}^*,\mathbf{\Psi}^*,\mathbf{\Psi}^*])$.

ALGORITHM III. FASTMER for SNR improvement.

Input:
    Fully sampled k-space of $\mathbf{x}$: $\mathbf{z}$; Tuning constants: λ_1, λ_2
    Number of k-space samples added at each iteration: N_k
    Expected fidelity of measurements: $\mathbf{A}$
Output: Estimated image: $\hat{\mathbf{x}}$
Initialize:
    $\mathbf{W}_1 = \mathbf{I}$, $\mathbf{W}_2 = \mathbf{I}$;
Reconstruction:
    while $\mathbf{z} \neq \emptyset$ **do**
    Move N_k new samples to $\mathbf{y}$ from $\mathbf{z}$ according to distance from center of k-space.
    Weighted reconstruction: Estimate $\hat{\mathbf{x}}$ by solving Eq. (7)
    Update weights: Update $\mathbf{W}_1$ and $\mathbf{W}_2$ according to Eq. (A1)
    end while

ALGORITHM IV. SFISTA algorithm for solving Eq. (7).

Input:
    k-space measurements: $\mathbf{y}$
    Sparsifying transform operator: $\mathbf{\Psi}_3$
    Inverse sparsifying transform operator: $\mathbf{\Psi}_3^*$
    Fourier operator: $\mathbf{F}_3$
    Inverse Fourier operator: $\mathbf{F}_3^*$
    Expected fidelity of measurements: $\mathbf{A}$
    Tuning constants: $\lambda_1, \lambda_2, \mu$
    An upper bound: $L \geq \|\mathbf{A}\mathbf{F}_3\|_2^2 + \frac{\|\mathbf{W}_1\mathbf{\Psi}_3\|_2^2 + \|\mathbf{W}_2\mathbf{B}\|_2^2}{\mu}$
Output: Estimated image: $\hat{\mathbf{x}}$
Initialize:
    $\mathbf{x}_1 = \mathbf{z}_2 = \mathbf{F}_3^*\mathbf{y}$, $t_2 = 1$
Iterations:
    Step k: ($k \geq 2$) Compute
    $\nabla f(\mathbf{z}_k) = \mathbf{A}^*(\mathbf{F}_3^*(\mathbf{A}(\mathbf{F}_3\mathbf{z}_k - \mathbf{y})))$
    $\nabla g_{1\mu}(\mathbf{W}_1\mathbf{\Psi}_3\mathbf{x}_{k-1}) = \frac{1}{\mu}\mathbf{W}_1\mathbf{\Psi}_3^*(\mathbf{W}_1\mathbf{\Psi}_3\mathbf{x}_{k-1} - \Gamma_{\lambda_1\mu}(\mathbf{W}_1\mathbf{\Psi}_3\mathbf{x}_{k-1}))$
    $\nabla g_{2\mu}(\mathbf{W}_2\mathbf{B}\mathbf{x}_{k-1}) = \frac{1}{\mu}\mathbf{W}_2\mathbf{B}(\mathbf{W}_2\mathbf{B}\mathbf{x}_{k-1} - \Gamma_{\lambda_2\mu}(\mathbf{W}_2\mathbf{B}\mathbf{x}_{k-1}))$
    $\mathbf{x}_k = \mathbf{z}_k - \frac{1}{L}(\nabla f(\mathbf{z}_k) + \nabla g_{1\mu}(\mathbf{W}_1\mathbf{\Psi}_3\mathbf{x}_{k-1}) + \nabla g_{2\mu}(\mathbf{W}_2\mathbf{B}\mathbf{x}_{k-1}))$
    $t_{k+1} = \frac{1+\sqrt{1+4t_k^2}}{2}$

T2-FLAIR experiment

Normalized difference image   Resulting $\mathbf{W}_1$ Resulting $\mathbf{W}_2$
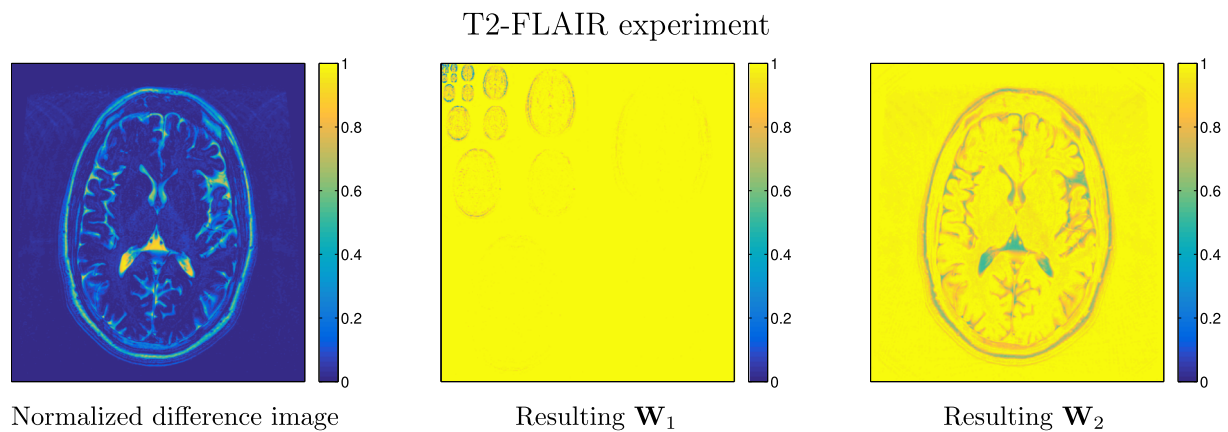
FIG. 5. T2-FLAIR experiment: Normalized difference image between the gold-standard FLAIR image and the reference T2-weighted image, and the resulting weighting matrices, $\mathbf{W}_1$ and $\mathbf{W}_2$ of FASTMER.

APPENDIX B: SIMILARITY MAPS AND RESULTING WEIGHTING MATRICES

In this appendix we present the similarity maps between each gold-standard to the reference image and the resulting weighting matrices, $\mathbf{W}_1$ and $\mathbf{W}_2$ for the cases examined in this paper. Note that although $\mathbf{x}$ is defined as a vector and the weighting matrices are defined as diagonal matrices, $\mathbf{W}_1$ and $\mathbf{W}_2$ are represented in this section as nondiagonal matrices, used to weight $\mathbf{x}$ represented as a 2D matrix, for convenience. In addition, the difference images refer to the absolute normalized difference.

Figures 5 and 6 show the maps for the T2-FLAIR and follow-up experiments and Fig. 7 shows the maps for the SNR improvement experiment. Here the difference map is computed between the input noisy adjacent slices. It can be seen that $\mathbf{W}_1$ converges to an inverse image of the wavelet transform of $\mathbf{X}$ and $\mathbf{W}_2$ converges to an inverse of the difference between $\mathbf{X}$ and $\mathbf{X}_0$, subject to minor changes due to the fact that $\mathbf{W}_i$ is forced to values between 0 and 1 and is based on computation from undersampled data. This convergence is successful since image quality improves as iterations progress (thanks to the addition of samples and the convergence of the algorithm).

APPENDIX C: METHOD PERFORMANCE FOR VARYING DEGREES OF SIMILARITY WITH THE REFERENCE IMAGE

To examine the performance of FASTMER for varying degrees of similarity between the reference image and the acquired image we repeated the experiment described in Sec. 4.A for misregistered reference image. Three scenarios were examined: 5° intraplane rotation, 45° intraplane rotation, and 5 mm interplane translation together with 5° rotation. The results are shown in Table II, while the gold-standard, wavelet+TV and FASTMER results without misregistration are given Fig. 1.

It can be seen that the images of FASTMER converge to that of TV+wavelet when a severe misregistration of 45° exists. This is indeed expected: FASTMER ignores the reference due to major changes between the reference and the acquired image. Rotation of 5° provides an improved reconstruction of PSNR = 32 dB, while a minor rotation and a 5 mm translation provides results which are slightly better than the wavelet+TV reconstruction. The results of this experiment support the assumption described in the paper, that high degree of similarity with the reference image provides better results and vice versa.

Follow-up experiment

Normalized difference image   Resulting $\mathbf{W}_1$ Resulting $\mathbf{W}_2$
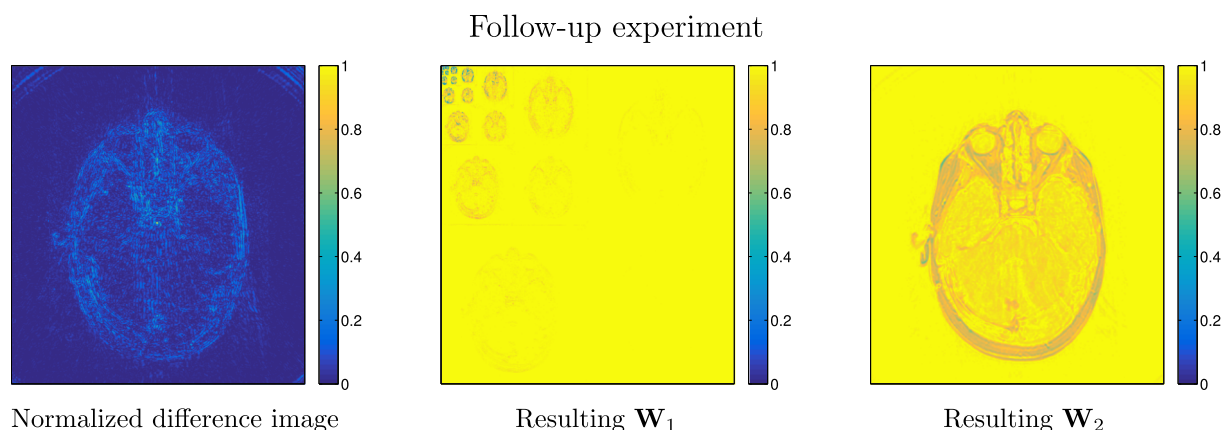
FIG. 6. Follow up experiment: Normalized difference image between the gold-standard follow-up image and the reference baseline image, and the resulting weighting matrices, $\mathbf{W}_1$ and $\mathbf{W}_2$ of FASTMER.
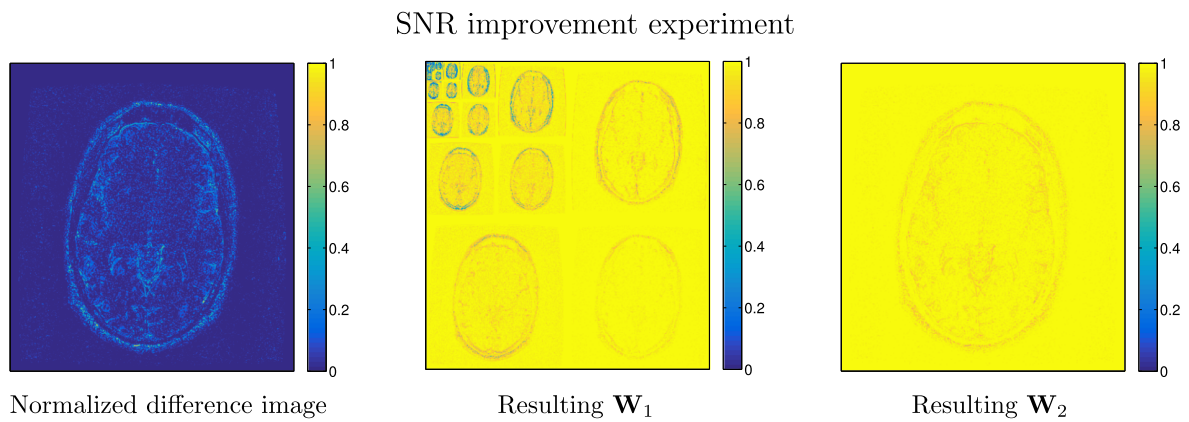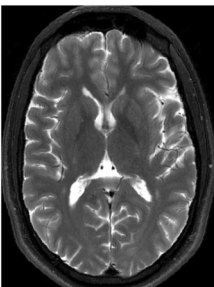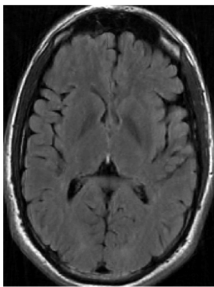
SNR improvement experiment

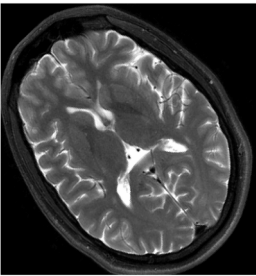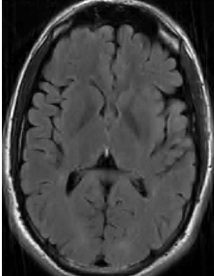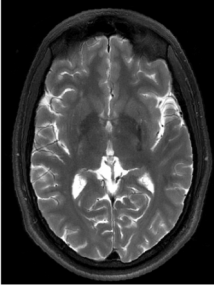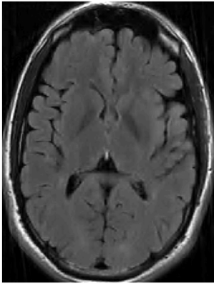| Normalized difference image | Resulting $\mathbf{W}_1$ | Resulting $\mathbf{W}_2$ |

FIG. 7. SNR improvement experiment: Normalized difference image between the two adjacent, low SNR input slices, and the resulting weighting matrices, $\mathbf{W}_1$ and $\mathbf{W}_2$ of FASTMER.

TABLE II. FASTMER results at various degrees of similarity with the reference image.

Misregistration description	Image used as a reference	FASTMER results	PSNR (dB)
Rotation of 5°			32
Rotation of 45°			28
Rotation of 5° + interplane translation of 5 mm			29

[a]Author to whom correspondence should be addressed. Electronic mail: weizmanl@tx.technion.ac.il; Telephone: +972-4-8291724.

[1]E. J. Candès, "Compressive sampling," in *Proceedings oh the International Congress of Mathematicians: Madrid, August 22-30, 2006: invited lectures* (2006), pp. 1433–1452.

[2]D. L. Donoho, "Compressed sensing," IEEE Trans. Inf. Theory **52**(4), 1289–1306 (2006).

[3]Y. C. Eldar and G. Kutyniok, *Compressed Sensing: Theory and Applications* (Cambridge University Press, Cambridge, UK, 2012).

[4]Y. C. Eldar, *Sampling Theory: Beyond Bandlimited Systems* (Cambridge University Press, Cambridge, UK, 2015).

[5]M. Lustig, D. Donoho, and J. M. Pauly, "Sparse MRI: The application of compressed sensing for rapid MR imaging," Magn. Reson. Med. **58**(6), 1182–1195 (2007).

[6]S. Ma, W. Yin, Y. Zhang, and A. Chakraborty, "An efficient algorithm for compressed MR imaging using total variation and wavelets," in *CVPR 2008, IEEE Conference on Computer Vision and Pattern Recognition* (IEEE, 2008), pp. 1–8.

[7]S. Ravishankar and Y. Bresler, "MR image reconstruction from highly undersampled *k*-space data by dictionary learning," IEEE Trans. Med. Imaging **30**(5), 1028–1041 (2011).

[8]X. Qu, D. Guo, B. Ning, Y. Hou, Y. Lin, S. Cai, and Z. Chen, "Undersampled MRI reconstruction with patch-based directional wavelets," Magn. Reson. Imaging **30**(7), 964–977 (2012).

[9]J. Caballero, A. N. Price, D. Rueckert, and J. V. Hajnal, "Dictionary learning and time sparsity for dynamic mr data reconstruction," *IEEE Trans. Med. Imaging* **33**(4), 979–994 (2014).

[10]Z.-P. Liang and P. C. Lauterbur, "A generalized series approach to MR spectroscopic imaging," *IEEE Trans. Med. Imaging* **10**(2), 132–137 (1991).

[11]J. M. Hanson, Z.-P. Liang, E. C. Wiener, and P. C. Lauterbur, "Fast dynamic imaging using two reference images," *Magn. Reson. Med.* **36**(1), 172–175 (1996).

[12]C. P. Hess, Z.-P. Liang, and P. C. Lauterbur, "Maximum cross-entropy generalized series reconstruction," *Int. J. Imaging Syst. Technol.* **10**(3), 258–265 (1999).

[13]S. Yun, S. S. Oh, Y. Han, and H. Park, "High-resolution fMRI with higher-order generalized series imaging and parallel imaging techniques (hgs-parallel)," *J. Magn. Reson. Imaging* **29**(4), 924–936 (2009).

[14]H. M. Nguyen and G. H. Glover, "A modified generalized series approach: Application to sparsely sampled fMRI," *IEEE Trans. Biomed. Eng.* **60**(10), 2867–2877 (2013).

[15]J. P. Haldar, V. J. Wedeen, M. Nezamzadeh, G. Dai, M. W. Weiner, N. Schuff, and Z.-P. Liang, "Improved diffusion imaging through SNR-enhancing joint reconstruction," *Magn. Reson. Med.* **69**(1), 277–289 (2013).

[16]M. Lustig, J. M. Santos, D. L. Donoho, and J. M. Pauly, "*K-T* sparse: High frame rate dynamic MRI exploiting spatio-temporal sparsity," in *Proceedings of the 13th Annual Meeting of ISMRM, Seattle* (Berkeley, CA, 2006), Vol. 2420.

[17]T. Lang and J. Ji, "Accelerating dynamic contrast-enhanced MRI using compressed sensing," in *Proceedings of the 16th annual meeting of ISMRM, Toronto, Canada* (Berkeley, CA, 2008), p. 1481.

[18]U. Gamper, P. Boesiger, and S. Kozerke, "Compressed sensing in dynamic MRI," *Magn. Reson. Med.* **59**(2), 365–373 (2008).

[19]H. Jung, K. Sung, K. S. Nayak, E. Y. Kim, and J. C. Ye, "*k-t* focuss: A general compressed sensing framework for high resolution dynamic MRI," *Magn. Reson. Med.* **61**(1), 103–116 (2009).

[20]L. Chen, A. Samsonov, and E. V. R. DiBella, "A framework for generalized reference image reconstruction methods including hypr-lr, pr-focuss, and *k-t* focuss," *J. Magn. Reson. Imaging* **34**(2), 403–412 (2011).

[21]M. Chiew, S. M. Smith, P. J. Koopmans, N. N. Graedel, T. Blumensath, and K. L. Miller, "*k-t* faster: Acceleration of functional MRI data acquisition using low rank constraints," *Magn. Reson. Med.* **74**, 353–364 (2014).

[22]G. Adluru, Y. Gur, L. Chen, D. Feinberg, J. Anderson, and E. V. R. DiBella, "MRI reconstruction of multi-image acquisitions using a rank regularizer with data reordering," *Med. Phys.* **42**(8), 4734–4744 (2015).

[23]R. Otazo, E. Candès, and D. K. Sodickson, "Low-rank plus sparse matrix decomposition for accelerated dynamic MRI with separation of background and dynamic components," *Magn. Reson. Med.* **73**(3), 1125–1136 (2015).

[24]B. Wu, R. P. Millane, R. Watts, and P. J. Bones, "Prior estimate-based compressed sensing in parallel MRI," *Magn. Reson. Med.* **65**(1), 83–95 (2011).

[25]X. Peng, H.-Q. Du, F. Lam, S. D. Babacan, and Z.-P. Liang, "Reference-driven MR image reconstruction with sparsity and support constraints," in *IEEE International Symposium on Biomedical Imaging: From Nano to Macro* (IEEE, NJ, 2011), pp. 89–92.

[26]H. Du and F. Lam, "Compressed sensing MR image reconstruction using a motion-compensated reference," *Magn. Reson. Imaging* **30**(7), 954–963 (2012).

[27]F. Lam, J. P. Haldar, and Z.-P. Liang, "Motion compensation for reference-constrained image reconstruction from limited data," in *IEEE International Symposium on Biomedical Imaging: From Nano to Macro* (IEEE, NJ, 2011), pp. 73–76.

[28]B. Bilgic, V. K. Goyal, and E. Adalsteinsson, "Multi-contrast reconstruction with bayesian compressed sensing," *Magn. Reson. Med.* **66**(6), 1601–1615 (2011).

[29]X. Qu, Y. Hou, F. Lam, D. Guo, and Z. Chen, "Magnetic resonance image reconstruction using similarities learnt from multi-modal images," in *IEEE China Summit & International Conference on Signal and Information Processing (ChinaSIP)* (IEEE, NJ, 2013), pp. 264–268.

[30]X. Qu, Y. Hou, F. Lam, D. Guo, J. Zhong, and Z. Chen, "Magnetic resonance image reconstruction from undersampled measurements using a patch-based nonlocal operator," *Med. Image Anal.* **18**(6), 843–856 (2014).

[31]J. Huang, C. Chen, and L. Axel, "Fast multi-contrast MRI reconstruction," *Magn. Reson. Imaging* **32**(10), 1344–1352 (2014).

[32]J. Tsao, B. Behnia, and A. G. Webb, "Unifying linear prior-information-driven methods for accelerated image acquisition," *Magn. Reson. Med.* **46**(4), 652–660 (2001).

[33]A. A. Samsonov, J. Velikina, J. O. Fleming, M. L. Schiebler, and A. S. Filed, "Accelerated serial MR imaging in multiple sclerosis using baseline scan information," in *Proceedings of the 18th annual meeting of ISMRM, Stockholm, Sweden* (Berkeley, CA, 2010), p. 4876.

[34]G. Li, Jürgen Hennig, E. Raithel, M. Büchert, D. Paul, J. G. Korvink, and M. Zaitsev, "Incorporation of image data from a previous examination in 3d serial MR imaging," *Magn. Reson. Mater. Phys., Biol. Med.* **28**, 413–425 (2015).

[35]X. Hu, D. N. Levin, P. C. Lauterbur, and T. Spraggins, "Slim: Spectral localization by imaging," *Magn. Reson. Med.* **8**(3), 314–322 (1988).

[36]G. Gindi *et al.*, "Bayesian reconstruction of functional images using anatomical information as priors," *IEEE Trans. Med. Imaging* **12**(4), 670–680 (1993).

[37]X. Ouyang, W. H. Wong, V. E. Johnson, X. Hu, and C.-T. Chen, "Incorporation of correlated structural images in pet image reconstruction," *IEEE Trans. Med. Imaging* **13**(4), 627–640 (1994).

[38]S. Somayajula, C. Panagiotou, A. Rangarajan, Q. Li, S. R. Arridge, and R. M. Leahy, "Pet image reconstruction using information theoretic anatomical priors," *IEEE Trans. Med. Imaging* **30**(3), 537–549 (2011).

[39]G.-H. Chen, J. Tang, and S. Leng, "Prior image constrained compressed sensing (piccs): A method to accurately reconstruct dynamic CT images from highly undersampled projection data sets," *Med. Phys.* **35**(2), 660–663 (2008).

[40]L. Weizman, Y. C. Eldar, and D. B. Bashat, "Compressed sensing for longitudinal MRI: An adaptive weighted approach," *Med. Phys.* **42**(9), 5195–5208 (2015).

[41]S. Ravishankar and Y. Bresler, "Adaptive sampling design for compressed sensing MRI," in *Annual International Conference of the IEEE Engineering in Medicine and Biology Society* (IEEE, NJ, 2011), pp. 3751–3755.

[42]L. Weizman, O. Rahamim, R. Dekel, Y. C. Eldar, and D. Ben-Bashat, "Exploiting similarity in adjacent slices for compressed sensing MRI," in *36th Annual International Conference of the IEEE Engineering in Medicine and Biology Society (EMBC), 2014* (IEEE, NJ, 2014), pp. 1549–1552.

[43]L. Weizman, Y. C. Eldar, A. Eilam, S. Londner, M. Artzi, and D. Ben Bashat, "Fast reference based MRI," in *37th Annual International Conference of the IEEE Engineering in Medicine and Biology Society (EMBC)* (IEEE, NJ, 2015), pp. 7486–7489.

[44]Z.-P. Liang and P. C. Lauterbur, "An efficient method for dynamic magnetic resonance imaging," *IEEE Trans. Med. Imaging* **13**(4), 677–686 (1994).

[45]J. Tsao, P. Boesiger, and K. P. Pruessmann, "*k-t* BLAST and *k-t* sense: Dynamic MRI with high frame rate exploiting spatiotemporal correlations," *Magn. Reson. Med.* **50**(5), 1031–1042 (2003).

[46]J. P. Haldar, D. Hernando, S.-K. Song, and Z.-P. Liang, "Anatomically constrained reconstruction from noisy data," *Magn. Reson. Med.* **59**(4), 810–818 (2008).

[47]E. J. Candès, M. B. Wakin, and S. P. Boyd, "Enhancing sparsity by reweighted l1 minimization," *J. Fourier Anal. Appl.* **14**(5-6), 877–905 (2008).

[48]Z. Tan, Y. C. Eldar, A. Beck, and A. Nehorai, "Smoothing and decomposition for analysis sparse recovery," *IEEE Trans. Signal Process.* **62**(7), 1762–1774 (2014).

[49]J. A. Fessler and B. P. Sutton, "Nonuniform fast fourier transforms using min-max interpolation," *IEEE Trans. Signal Process.* **51**(2), 560–574 (2003).

[50]J. F. C. Mota, L. Weizman, N. Deligiannis, Y. C. Eldar, and M. R. D. Rodrigues, "Reference-based compressed sensing: A sample complexity approach," in *IEEE International Conference on Acoustics, Speech and Signal Processing (ICASSP)* (IEEE, NJ, 2016), pp. 4687–4691.

[51]G. P. Zientara, L. P. Panych, and F. A. Jolesz, "Dynamically adaptive MRI with encoding by singular value decomposition," *Magn. Reson. Med.* **32**(2), 268–274 (1994).

[52]S. K. Nagle and D. N. Levin, "Multiple region MRI," *Magn. Reson. Med.* **41**(4), 774–786 (1999).

[53]Y. Gao and S. J. Reeves, "Optimal *k*-space sampling in MRSI for images with a limited region of support," *IEEE Trans. Med. Imaging* **19**(12), 1168–1178 (2000).

[54]J. Haupt, R. Nowak, and R. Castro, "Adaptive sensing for sparse signal recovery," in *IEEE 13th Digital Signal Processing Workshop and 5th IEEE Signal Processing Education Workshop, DSP/SPE 2009* (IEEE, NJ, 2009), pp. 702–707.

[55]J. Haupt, R. M. Castro, and R. Nowak, "Distilled sensing: Adaptive sampling for sparse detection and estimation," IEEE Trans. Inf. Theory **57**(9), 6222–6235 (2011).

[56]D. Wei and A. O. Hero, "Multistage adaptive estimation of sparse signals,"

IEEE J. Sel. Top. Signal Process. **7**(5), 783–796 (2013).

[57]M. Seeger, H. Nickisch, R. Pohmann, and B. Schölkopf, "Optimization of *k*-space trajectories for compressed sensing by bayesian experimental design," Magn. Reson. Med. **63**(1), 116–126 (2010).

[58]J. Song, Y. Liu, S. L. Gewalt, G. Cofer, G. A. Johnson, and Q. H. Liu, "Least-square nufft methods applied to 2-d and 3-d radially encoded mr image reconstruction," IEEE Trans. Biomed. Eng. **56**(4), 1134–1142 (2009).